RESEARCH ARTICLE

ESPL **WILEY**

Sounding out the river: Seismic and hydroacoustic monitoring of bedload transport

Bronwyn Matthews[1] | Mark Naylor[1] | Hugh Sinclair[1] | Andrew Black[2] | Richard Williams[3] | Calum Cuthill[1,4] | Matthew Gervais[1] | Michael Dietze[5,6] | Anna Smith[1]

[1]School of GeoSciences, University of Edinburgh, Edinburgh, UK

[2]School of Humanities, Social Sciences and Law, University of Dundee, Dundee, UK

[3]School of Geographical & Earth Sciences, University of Glasgow, Glasgow, UK

[4]School of Engineering, University of Glasgow, Glasgow, UK

[5]Geographical Institute, Georg-August University Göttingen, Göttingen, Germany

[6]Geomorphologie, GFZ Potsdam, Potsdam, Germany

Correspondence

Bronwyn Matthews, School of Geosciences, University of Edinburgh, Edinburgh EH8 9XP, UK.
Email: bronwyn.matthews@ed.ac.uk

Abstract

Seismological observations provide a non-invasive and continuous means for indirectly measuring fluvial bedload transport. A significant challenge remains in independently characterising the seismic signature of bedload transport from other sources such as turbulence. We present a unique dataset from an alluvial Scottish river, combining seismic data and hydroacoustic measurements, to analyse bedload transport during three high-flow events occurring within the same year. By studying three successive events, we assess the consistency of bedload transport thresholds in response to changing flow conditions and explore the presence of hysteresis in seismic data versus water level as an indicator of coarse bedload transport. Through the use of hydroacoustic data to independently characterise bedload transport, our findings reveal that bedload transport occurred during all three events but that the threshold for entrainment varied. These entrainment thresholds were influenced by antecedent events, with a drop of 15%–20% of the threshold flow depth following the largest of the three events. In agreement with recent studies, we also found that hysteresis in the seismic versus water level data is not sufficient for identifying and analysing bedload transport: Distinct hysteresis was only observed during the largest of the three events despite all events experiencing bedload transport as observed through the independent hydroacoustic data. Our work shows the value in combining independent datasets for long-term monitoring of bedload transport to understand the evolution in the thresholds of bedload motion, providing crucial information for effective river and land-use management in a changing climate with potentially impacted high-flow events.

KEYWORDS

bedload transport, entrainment threshold, environmental seismology, fluvial geomorphology, river

1 | INTRODUCTION

Intensification of flood events linked to climate and land-use change poses significant threats to both infrastructure and ecosystems in many areas across the world. Climate change can drive increases in flood frequency and intensity, leading to increased transport of sediment and debris by rivers. Flooding and the transport of coarse gravelly bedload can benefit aquatic ecosystems; however, increased magnitude and frequency of flooding could have profound ecological consequences, altering riverbed morphology, disturbing aquatic habitats and negatively impacting aquatic species (Hauer et al., 2018). The transport of bedload can also have significant impacts on infrastructure such as bridges and dams causing erosion and scour (Church, 2006; Roth et al., 2017; Turowski et al., 2011). Additionally,

3840 | wileyonlinelibrary.com/journal/esp

Earth Surf. Process. Landforms. 2024;49:3840–3854.

anthropogenic activities, including urban development, deforestation, channelisation and re-naturalisation for river management purposes, alter the patterns of bedload transport in rivers (Cox et al., 2021). Therefore, monitoring and understanding the timing and characteristics of coarse sediment mobilisation are crucial for predicting changes in channel morphology. This knowledge is essential for various applications, including designing and maintaining infrastructure to resist fluvial erosion, improving flood management, optimising sustainable water resource use and preserving aquatic ecosystem health.

The dynamic and destructive nature of sediment movement in rivers makes monitoring and measuring the transport of coarse bedload challenging, particularly as rivers erode and aggrade their bed and shift their course. One of the key challenges lies in accurately measuring the onset of entrainment of bedload and the continuous measurement of bedload transport in rivers. Variations in entrainment thresholds are influenced by factors such as particle shape and size distribution (Jain et al., 2021; Wilcock & Crowe, 2003), bedforms (Church et al., 1998), sediment cohesion (Kothyari & Jain, 2008) and changes in grain size between the bed surface and subsurface where coarse sediment may act to armour the river bed (Jain et al., 2021; Lisle & Madej, 1992). Tracer experiments that use pebbles loaded with accelerometers have demonstrated the complexity of entrainment thresholds with both clockwise and anticlockwise hysteresis between seismic power and streamflow during floods (Pretzlav et al., 2020). Using flume tank experiments, it has been demonstrated that variations in bedload transport entrainment respond to durations and frequencies of moderate to peak discharge conditions, as a result of the river bed surface becoming more or less stable (Luo et al., 2023; Ockelford et al., 2019). The grain size distribution may be modified at the bed surface by winnowing of finer grains, resulting in the formation of an armoured surface layer of coarser grains (Gomez & Soar, 2022; Pitlick et al., 2009). This armouring modifies the onset of bedload entrainment complicating the relationship between the measured grain size distribution and the entrainment threshold. A further complication to the measurement of bedload transport is the hysteresis patterns, where sediment transport rates do not have a linear scaling with the flow conditions (Bogen, 1980). Armouring is an example of a process that could result in hysteresis in bedload transport as it may increase the threshold for sediment motion on the bed, causing the rising and falling limbs of a flood hydrograph to have different threshold entrainment values. The mobilisation of coarse bedload can also be influenced by the suspended sediment concentration at the sediment water interface (An et al., 2018; Rickenmann, 1991). Suspended sediment loads are commonly higher during the rising limb of flood hydrographs that also results in different entrainment thresholds on either side of a flood. Another potential driver of hysteresis relates to the history of large events that reorganise the bed and change the critical shear stress for subsequent events (Masteller et al., 2019; Turowski et al., 2011). The range of variables that determine entrainment thresholds as outlined above are also reflected in variations in dimensionless critical shear stress values of median grain sizes synthesised from a range of settings (e.g. Buffington & Montgomery, 1997).

Addressing the challenges of determining bedload entrainment thresholds for a given location requires innovative site and reach-scale measurement techniques. This facilitates a more comprehensive understanding of bedload transport dynamics and the interplay between sediments, flow dynamics and riverbed characteristics. However, since coarse bedload is mobilised when rivers are at high flow, logistical challenges are introduced when using many commonly used measurement techniques. Traditional methods of monitoring bedload transport in rivers, such as sediment sampling, sediment traps, grain size analysis and flow measurements, have typically relied on direct field measurements and observations and have been successfully used in a number of places, particularly in documenting the early motion of small grain sizes (Bunte et al., 2004; Habersack et al., 2001; Holmes, 2010; Reid et al., 1985). However, these approaches come with several limitations: sediment sampling and flow measurements can be labour intensive, time consuming and difficult at high flows, while sediment traps (although continuous in measurement) are limited by the rapid filling of traps in high bedload transport rivers and the upper limit of grain sizes that can be measured as a result of the trap size. This limitation means they are less applicable to rivers with high sediment transport rates of large cobble to boulder sized bedload (Bunte & Abt, 2005; Bunte et al., 2004; Thorne, 2014). Non-continuous traditional methods struggle to capture the full complexity and natural dynamics of bedload transport, as they are typically performed during modest hydrologic events, over short timescales and during daylight hours. Although some studies have used bedload samplers deployed across entire cross sections of rivers (e.g. Dietze et al., 2019), these methods generally only measure at a single point in space, while bedload transport occurs along cross-sections with potentially variable transport at individual points in space. As a result, they may not provide sufficiently representative data needed for effective river management, infrastructure design or understanding sediment transport patterns. Tracer grains have also enabled insight into these processes (e.g. Pretzlav et al., 2020) but are again challenging when large-scale bedload movement is involved that disperses and buries the tracers long distances downstream. Engineers often use numerical models or empirical equations as alternatives to traditional methods for predicting bedload transport (Geay et al., 2020). However, simplification of these empirical equations relative to complexities of natural bedload transport processes in rivers—and the challenge of estimating grain size distribution, entrainment thresholds and bed morphology, among other factors—results in considerable uncertainties in the sediment transport predictions (Dey, 2014; Downs et al., 2016).

New measurement techniques are increasingly being employed to address these limitations and provide more precise insights into bedload transport dynamics. Several recent studies have explored the potential for seismic sensors (such as geophones) to monitor environmental and geomorphic processes (e.g. Burtin et al., 2008; Dietze & Gimbert, 2019; Lagarde et al., 2021; Roth et al., 2016). Geophones, which are typically used for seismic studies, have important applications in the field of bedload transport monitoring. Previously, impact plate geophones have been strategically deployed in riverbeds to measure impacts on the bed (e.g. Downs et al., 2016; Rickenmann et al., 2014; Rickenmann et al., 2022), and seismic geophones have been deployed on river banks to capture the ground vibrations caused by bedload particles interacting with the river bed (e.g. Barrière et al., 2015; Burtin et al., 2008; Schmandt et al., 2013). These vibrations can be analysed to estimate the timings, intensity and frequency of bedload transport in rivers. This innovative use of geophones provides a non-intrusive and continuous monitoring method that

overcomes some limitations associated with traditional bedload measurement techniques, facilitating the monitoring of bedload transport under conditions that were previously not possible (Burtin et al., 2010). Geophones record a range of environmental signals that are filtered by their passage through the subsurface. The potential sources for these signals include precipitation, wind, tides, traffic, turbulent motion in rivers and the impact of bedload on riverbeds (Burtin et al., 2008; Rindraharisaona et al., 2022; Wilcock et al., 1999). Previous studies have focused on the frequency characteristics of seismic energy to discriminate different sources of seismic noise (Burtin et al., 2008; Burtin et al., 2014; Gimbert et al., 2014). The key discrimination for river-induced seismic signals is between coarse bedload transport and water turbulence. It has been suggested that bedload transport induces broadband higher frequency seismic waves than the continuous signal from river turbulence (Gimbert et al., 2014; Schmandt et al., 2013; Vore et al., 2019). Tsai et al. (2012) and Gimbert et al. (2014) developed a physical inversion model that inverts recorded river seismic signals using field observations such as ground seismic properties and grain size distributions to estimates of bedload transport and water depth. Many studies have successfully utilised and edited this model to provide these estimates in a range of fluvial settings (e.g. Bakker et al., 2020; Dietze & Gimbert, 2019). However, due to the overlap in bedload and turbulence frequency bands observed in these studies, it makes it difficult to accurately differentiate between the signal sources.

By correlating the bedload induced seismic data with river discharge, crucial insights have been gained into the dynamics of sediment transport and how it responds to variations in hydraulic characteristics. Many studies found a hysteretic relationship between these parameters that have been interpreted to be evidence of bedload transport, as significant hysteresis is not expected in the relationship between river stage and turbulence (Hsu et al., 2011; Roth et al., 2016; Roth et al., 2017; Turowski et al., 2013). As outlined above, factors like particle size, shape and bed structure can influence the initiation of bedload transport on rivers, such that sediment entrainment thresholds may vary relative to changes in flow conditions. Bedload transport may even continue after the water level has decreased below the initial entrainment threshold or may initiate and cease at different levels, due to changes in the hydraulic characteristics of the channel as a result of deposition upstream or the formation of new bars, which can also affect the availability of sediment for mobilisation. This interpretation of hysteresis has become a foundational assumption for many fluvial seismic studies, with some studies reporting a clockwise pattern of hysteresis where bedload transport peaks before the peak in water level and some recording an anticlockwise pattern where the peak in water level occurs prior to the peak in bedload transport. Clockwise patterns are associated with readily available sediments (Gaeuman, 2010; Hassan et al., 2006; Kuhnle, 1992; Mao, 2012; Mao et al., 2014; Reid et al., 1985), while anticlockwise patterns are thought to be caused by processes that increase sediment supply after a flood peak (Kuhnle, 1992; Lee et al., 2004; Mao et al., 2014; Reid et al., 1985). These previous seismic studies (e.g. Chao et al., 2015; Hsu et al., 2011) have shed light on the invaluable use of geophones for bedload monitoring purposes; however, they generally had little independent data to constrain when bedload was being transported.

These uncertainties in the overlapping frequency bands of river-induced seismic signals and the assumptions in interpreting bedload transport processes using the relationship between seismic power and water level make the interpretation of bedload transport occurrence based on seismic data alone somewhat subjective. Therefore, it is beneficial to have an independent measure of bedload transport to cross-check with the seismic signals. To test some of the assumptions used in interpreting geophone data, we combine geophones deployed on riverbanks with acoustic hydrophones deployed in the water column to independently classify when coarse bedload is transported. Hydrophones have been used to detect and record underwater sound, making them particularly useful for applications in the fields of marine biology, underwater communication and sonar systems (Ballance et al., 2023; Bountourakis et al., 2023). Some previous bedload studies (e.g. Rickenmann et al., 2022; Stark et al., 2024) have used hydrophones that are deployed in pipes to record the sound of particle impacts with the instrument. However, in contrast to geophones, they can also be suspended in the water column to record the full acoustic signal of impacts between the particles and the bed as well as inter-particle collisions. These suspended acoustic hydrophones, herein referred to as acoustic hydrophones, are sensitive to even the interaction of sand particles in low flow and can therefore record collisions of the full range of particle sizes within the local river channel, making them a potentially very useful method for grain size analysis. However, it is logistically difficult to deploy acoustic hydrophones routinely as they have to be placed within a river water column for the duration of the measurements, thus requiring careful methodological approach and appropriate housing to protect the instrument during high-flow events (Osborne et al., 2021). On an event-by-event basis, they can provide independent data to critique the seismic bedload transport information obtained from geophones and to test whether hysteresis in the relationship between the fluvial seismic signal and water level is in fact a fingerprint of bedload transport.

Here, we use co-located acoustic hydrophones (https://jezrileyfrench.co.uk/hydrophones.php) to evaluate the application of geophone data in characterising the onset of coarse bedload transport and critique assumptions that use hysteresis as a characteristic of bedload transport from geophone data. Our study determines bedload mobilisation thresholds and evaluates the influence of antecedent events through independent seismic and hydroacoustic characterisations through multiple flood cycles. By integrating seismic, water level and hydroacoustic data, we aim to gain insights into bedload transport thresholds, examine hysteresis patterns and shed light on the intricate relationship between sediment transport and discharge. Our analysis focuses on a relatively stable section of the gravel-bed River Feshie in the Scottish Cairngorms (Figure 1) and analyses seismic signals from the three largest flow events in 2022. We explore how hydrographic sequencing (Ockelford et al., 2019; Ockelford & Haynes, 2013) at the River Feshie affects bedload transport entrainment thresholds through the independent analysis of seismic and hydroacoustic data.

2 | METHODS

2.1 | Field site: River Feshie

The River Feshie in Scotland is an alluvial tributary of the River Spey and drains a catchment of ~240 km² with a maximum elevation of
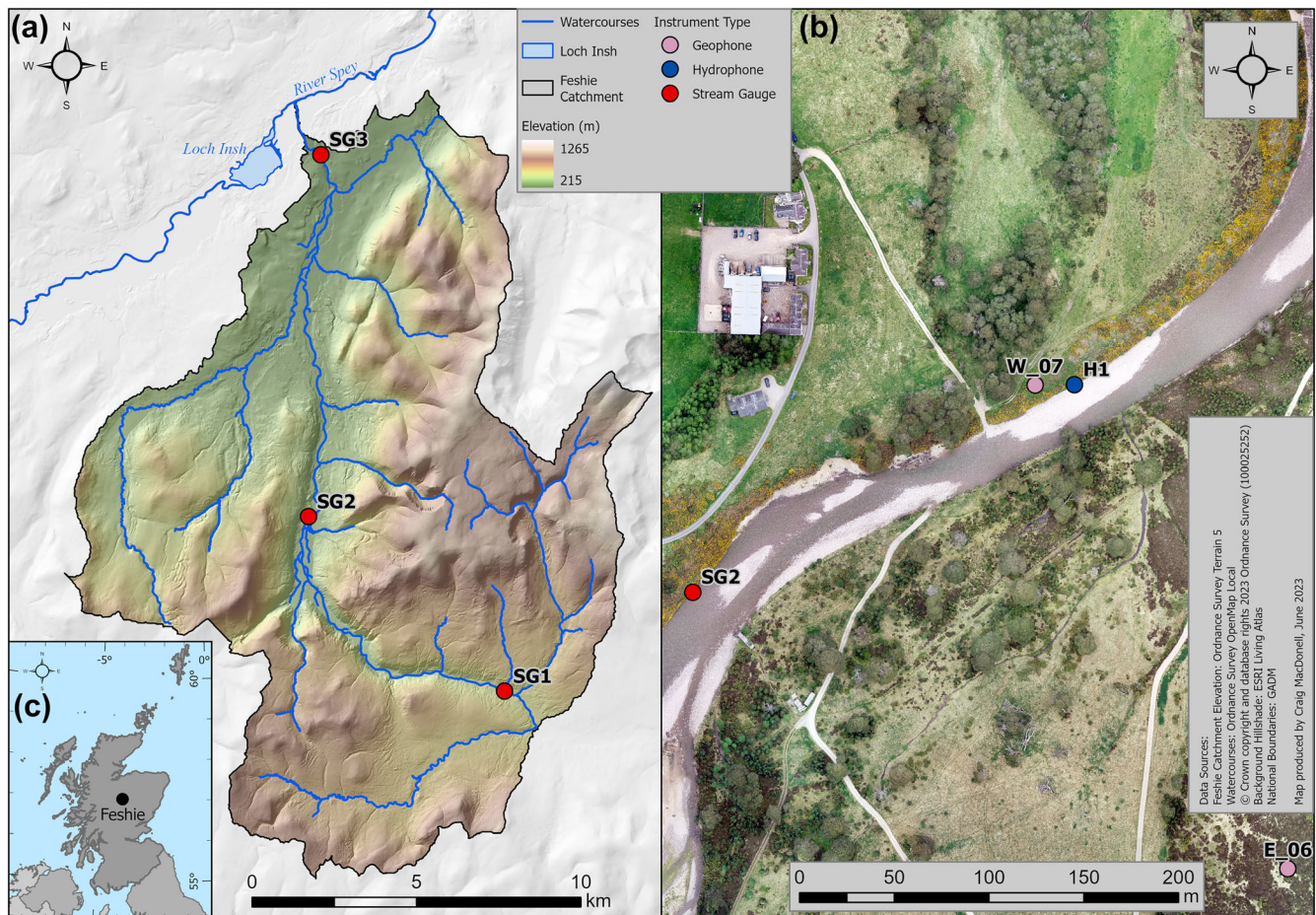
FIGURE 1 Maps of the River Feshie fieldsite at the (a) catchment scale showing the three stream gauge sites, (b) reach scale showing the sites of instruments used in this study and (c) national scale. Photos of the field deployments can be found in Supporting Information S1. [Color figure can be viewed at wileyonlinelibrary.com]

just over 1200 m (Figure 1) (Ferguson & Werritty, 1983). The bedrock has low permeability, which results in a hydrograph that is very responsive to rain and snowmelt events (Chełmicki & Krzemień, 1999). The headwaters sit on the peat-rich plateau of the Cairngorms (upstream of SG1 in Figure 1) and then flow downstream through glacial outwash gravels (downstream of SG1 in Figure 1). The Feshie is supplied largely by the erosion of glacial moraine and outwash channels, resulting in a broad, braided gravel-dominated river (Brasington et al., 2000; Ferguson & Werritty, 1983). We focus on a ~500 m long (Figure 1b), single-thread reach just downstream of a wide multi-thread braided section (Figures 1 and 2). Within the study site, the channel width varies from 25 to 70 m and has a local slope of ~0.006. The bedrock is predominantly Moinian schist and granite, which dominate the bedload (Ferguson & Werritty, 1983). The average grain sizes in the bar adjacent to the geophone station measured using the Wolman pebble count method (Wolman, 1954) routinely before and after the 2022 events ranged from 5 to 194 mm with specific grain size fractions: $D_{16} = 14$ mm, $D_{50} = 35$ mm and $D_{84} = 72$ mm.

A stream gauge that is currently located approximately 12 km downstream from our site at Feshiebridge (SG3 in Figure 1), maintained by the Scottish Environment Protection Agency (SEPA), records a variable flow regime with peak flows exceeding 100 m^{3}s^{-1} and a maximum peak flow of 260 m^{3}s^{-1} since recording began in December 1992. From flow data over the last 7 years at Feshiebridge

(SG3) (Figure 3a), it can be seen that there are generally larger flows occurring during winter and spring. Flow patterns of 2022 were generally similar to previous years with low flows during summer and larger peaked flows in spring, autumn and winter. Summer flows in 2022 were particularly low and were bounded by large events in early spring and autumn. The largest event of 2022, which we use for this analysis, peaked at around 138 m^{3}s^{-1} at SG3 in September. Prior to this, there had only been six other peaks that exceeded this level over 7 years (Figure 3a); the largest of these occurring in December 2015 as a result of Storm Frank that caused widespread flooding across much of Scotland, Northern England and Wales (Barker et al., 2016). Historically, in the late 1970s, a stream gauge was maintained in the same stretch as our study site by Ferguson & Werritty (1983) and recorded a mean flow of 3–4 m^{3}s^{-1} with regular floods reaching 20–30 m^{3}s^{-1} and the largest recorded floods exceeded 100 m^{3}s^{-1}.

2.2 | Data collection

2.2.1 | Stream gauge data

This study uses water level (stage) measurements recorded at three stream gauge sites on the River Feshie. To measure water level at our study site, we deployed a LiDAR (Light Detection and Ranging) water level sensor on the remains of a footbridge at site SG2, which
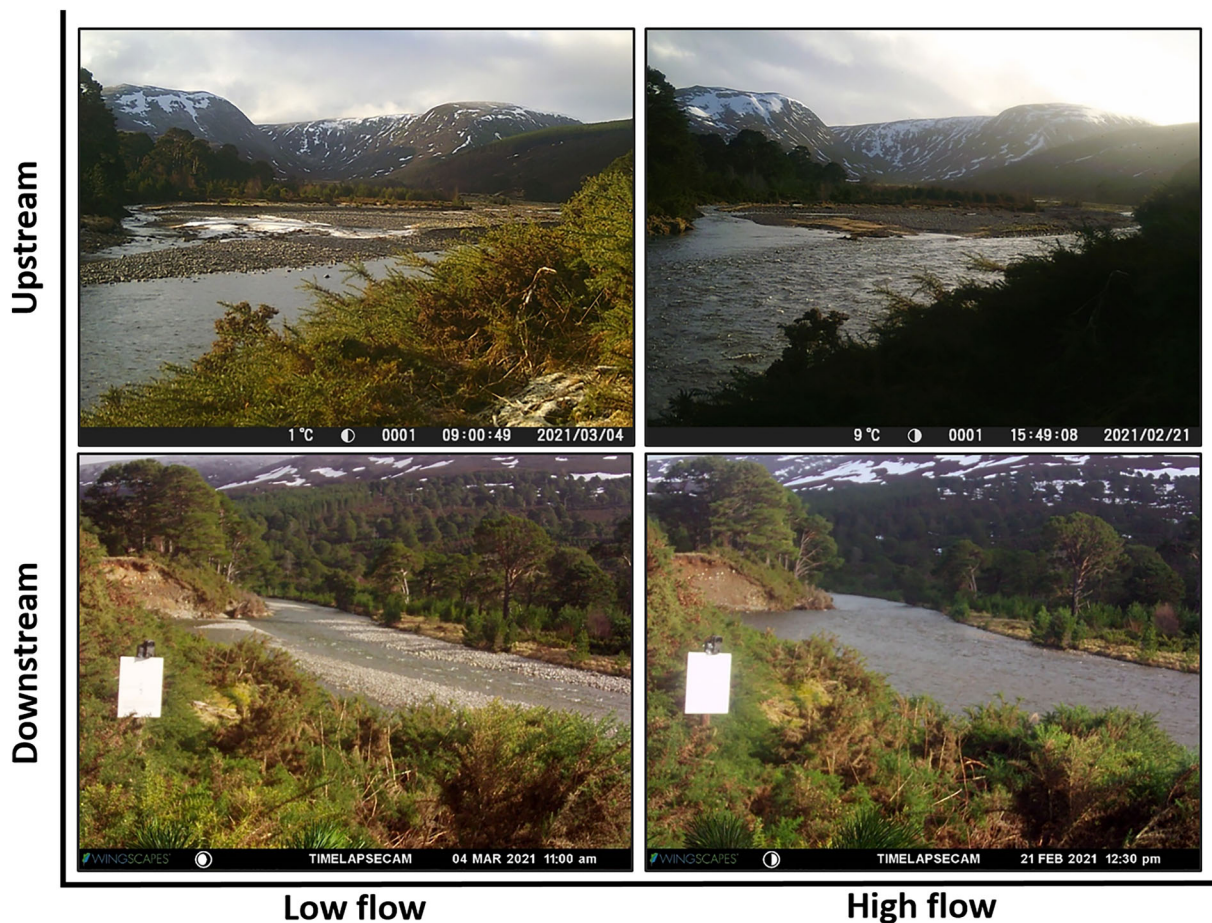
FIGURE 2 Photos from the River Feshie fieldsite looking upstream and downstream from SG2 during high flow and low flows. Images are taken from February and March 2021 as these had the clearest conditions and are representative of general high and low flows at the site. During the low-flow event, the SEPA stream gauge at SG3 measured a water level of 0.76 m and the high-flow event photographed here peaked at 2.15 m at SG3. [Color figure can be viewed at wileyonlinelibrary.com]

measures the distance to the water surface every 5 min. The water level data were corrected for the height of the sensor above the river-bed to provide approximate water depth measurements, assuming the river bed was fixed. Repeat measurements of the distance from the sensor to the river bed confirmed that the bed was stable at this location and the elevation of the bed remained constant during our study period. Although we can convert to water discharge using these data combined with channel geometry measurements, we do not have good constraints to accurately undertake this conversion, which would induce uncertainty and therefore have chosen to work with the primary water level observations. We also have access to water level and discharge data collected every 15 min at stream gauges SG1 and SG3, located approximately 10 km upstream and downstream of our site (Figure 1). These data are managed by Dr Andrew Black (University of Dundee) and SEPA, respectively. We use the SEPA data as the historic record, since our local sensor has only been operational since the end of 2020.

The three events analysed in this study occurred on the 11–14 March 2022 (three successive peaks with a maximum water level of 1.27 m at SG2), 30 September–1 October 2022 (one peak with a maximum water level of 1.69 m at SG2, a roughly once-in-a-year event) and 2–3 November 2022 (one peak with a maximum water level of 1.30 m at SG2). These events are herein referred to as the 'March event', the 'September–October event' and the 'November event',

respectively. The March event followed a series of snowmelt cycles that caused three repeated peaks in water level, resulting from rainfall on snow combined with snowmelt and peaked at 84 m^3s^{-1} at the SEPA station SG3. The larger September–October event was of a shorter duration and occurred following intense precipitation in the catchment that coincided with the tailend of Hurricane Fiona that hit Canada in mid-late September 2022, resulting in peak discharge of 138 m^3s^{-1} at SG3. The November event was an early winter storm with similar magnitude to the March event; however, it occurred as a result of high rainfall alone, reaching peak discharge at 90 m^3s^{-1}. The three peaks in the first event allow us to test the consistency of the onset of bedload, the second event allows us to explore the impact of a large event on these thresholds of motion, and the third event allows us to explore the new behaviour of the river after a large event. Thus, combining data from successive high-flow events, with only a few small scale peaks occurring in between (Figure 3b), demonstrates how the technique can be used to make inferences about the effects of antecedent events on the mobilisation of bedload.

2.2.2 | Seismic and hydroacoustic data

This study integrates seismic and hydroacoustic data to study the mobilisation and transport of bedload along a short (∼100 m) stretch
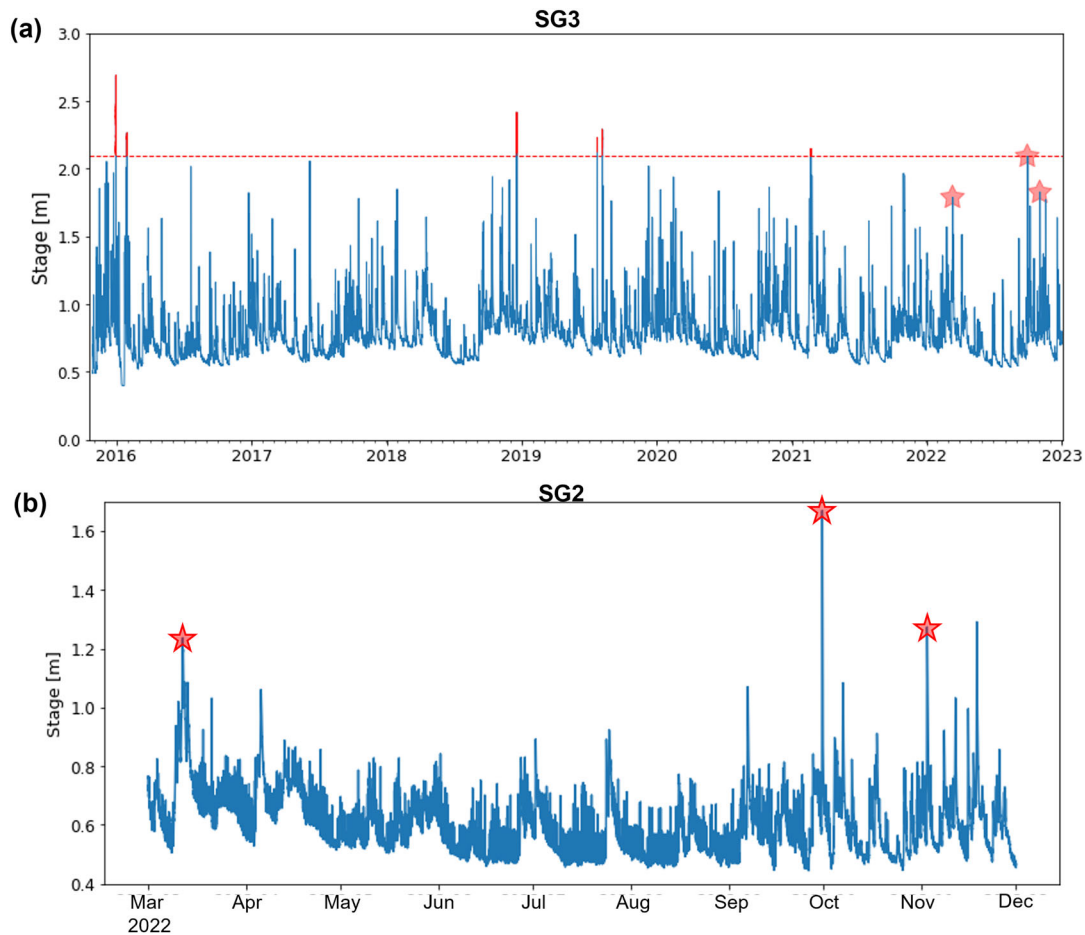
FIGURE 3 (a) Stage measurements from SEPA stream gauge at SG3 from 27 October 2015 to 31 December 2022. Red stars mark the three largest events in 2022 that are analysed in this study. Red line marks the water level of the largest event in 2022, with peaks that have previously exceeded this value also marked in red. (b) Stage measurements from local stream gauge sensor at SG2 from March through November 2022, showing the three largest events with the red stars. [Color figure can be viewed at wileyonlinelibrary.com]

of the River Feshie (Figure 1). We use the co-located stream gauge sensor (SG2) to analyse the dependence of the seismic and hydroacoustic data on water level.

We compare data from two three-component PE6B (4.5 Hz) geophones connected to Digos Data-Cube loggers recording at a sampling rate of 200 Hz. The geophone data were continuously recorded. The geophones were buried in soil at approximately 10 cm depth (base of instrument to surface), levelled and oriented with the north–south (horizontal) component aligned along the downstream river direction. The geophone at site W_07 was located within approximately 5 m of the river and 1 m above the base flow water surface. It was well sited to record a strong river signal as the small source-to-sensor distance minimises the attenuation of high frequencies, which is important for this study as we are wanting to resolve frequencies of bedload transport (Figure 1). The geophone at site E_06 was located approximately 300 m from the river as a control site to characterise other sources of environmental noise, such as precipitation and wind as the impact of rain on the ground and the movement of vegetation by wind can be recorded by geophones (Dean, 2018; Rindraharisaona et al., 2022). Both sites have similar geology with high-velocity Moinian schist bedrock overlain by low-velocity glacial till (Ferguson & Werritty, 1983). Signals are common to both W_07 and E_06 we identified as non-river environmental noise, and this approach allowed us to confirm that the relatively high broadband noise level prior to the water rising is due to hydrometeorological noise. Generally, seismic bedload studies have used the vertical component of seismic waves as, due to the impact direction of bedload on the river bed, it was assumed that the emitted seismic waves would be best represented by Rayleigh waves with strong vertical displacements (Dietze et al., 2019; Tsai et al., 2012). Here, we present the analysis of the stream-parallel component. This was chosen because, although using the vertical and the stream-perpendicular components for the analysis gave similar results, the vertical component tended to be noisier due to its susceptibility to rain interference (see Supporting Information S1) and theoretically the stream-parallel component should give the strongest river-related signal (Roth et al., 2016). The area is anthropogenically very quiet with little traffic on the estate roads, so there is minimal interference from these sources. The geophones are expected to record both the interaction of turbulence in the water with the bed and direct collisions of particles with the bed. It has previously been found that seismic waves emitted from bedload collisions resulted in higher frequencies than those from turbulence, with bedload generally found to occur in the range of 30–60 Hz and turbulence around 1–20 Hz (Dietze & Gimbert, 2019; Gimbert et al., 2014; Tsai et al., 2012). However, studies by Schmandt et al. (2013) and Schmandt et al. (2017) found that the bedload signals could be recorded in a range of frequencies from 15 to 100 Hz.

To independently characterise bedload motion recorded within the study site, we deployed a hydrophone (Jez Riley French D-series; https://jezrileyfrench.co.uk/hydrophones.php) within the river at site H1 connected to our own Raspberry Pi logger to record the hydroacoustic signal of turbulence and bedload motion. In previous hydroacoustic studies, hydrophones have been deployed in metal pipes or attached to metal plates embedded in the river bed (Barrière et al., 2015), attached to the bottom of boats or river surveying equipment such as river boards (Geay et al., 2020) or attached to man-made infrastructure, such as bridges or metal frames (Belleudy et al., 2010); however, this was logistically not an option in our study site. Instead, the hydrophone was mounted within a roughly 40 kg (0.4 × 0.3 × 0.3 m) granite block with a hollow cylindrical core of diameter 0.2 m in order to protect it from damage by direct impacts from mobile material (see Supporting Information S1). The hydrophone block was located approximately 5 m downstream of the geophone at site W_07 and 40 cm from the river bank (Figure 1). The recording system was built using a Pi Zero, a Witty Pi for scheduling and a HiFiBerry DAC + ADC Pro sound card (sampling at 44.1 kHz); due to the size of the datafiles, we recorded a 30-s sample every 15 min. Data were recorded at two different gains of 30 and 40 dB to manage potential issues of data quality. In addition to measuring collisions between particles and the bed, like geophones, acoustic hydrophones have the potential to record collisions of particles in suspension. The hydroacoustic data provide independent evidence of bedload motion within the channel. It was used as a complementary data set to the seismic data to confirm the occurrence and timing of bedload motion, which is challenging using seismic data alone due to the overlapping frequencies of bedload and turbulence signals, as well as other environmental noise.

2.3 | Data processing and analysis

We pre-process the seismic data by removing the instrument response through ObsPy using information provided by Digos on the specific instrument used. We then apply a bandpass filter in the frequency domain (between 4.5 and 99 Hz) to the data prior to deconvolution to remove the frequencies most affected by the instrument. The data is then detrended to remove the mean trend of the signal using ObsPy. We computed the power spectral density (PSD) using Welch's method (Welch, 1967) with a 1-min window and no overlap to quantify the variation in seismic power as a function of time and frequency, which we compare to water level. In order to isolate the bedload signal, the standard methodology is to then average the PSD over the relevant frequency bands (Bakker et al., 2020; Lagarde et al., 2021; Tsai et al., 2012). This frequency range is typically around 30–60 Hz with turbulence found to be approximately 1–20 Hz (Dietze & Gimbert, 2019; Gimbert et al., 2014; Tsai et al., 2012). This approach allows us to compute the PSD for the seismic energy recorded within the frequency range commonly associated with the occurrence of bedload transport. The data are plotted as a visual representation of the frequencies of the signal over time as a spectrogram and then as a time-varying PSD plot to show the temporal change in seismic power over the chosen frequency bands.

Here, we do not use the models developed by Tsai et al. (2012) and Gimbert et al. (2014) for our analysis as we wanted to take a data-driven approach. Although these models have been successfully used in other studies and calibrated with field and flume measurements (Bakker et al., 2020; Lagarde et al., 2021), we wanted to focus on the real data rather than applying a model to interpret our data and integrating assumptions into the analysis based on the model outputs. The structure of our data is more complicated than the models can handle and thus we believe it is important to interpret the real data.

The raw hydroacoustic data contain considerable information about the processes occurring in the river. There is a distinct audible signal from turbulence (gurgling), smaller grain sizes being transported (tinkling and tapping) and larger grain sizes being transported (thudding and knocking), which can be used to manually classify the dominant process (see Audio S2,S3,S4). For the duration of each of the three high-flow events considered here, the 30-s hydroacoustic recordings taken every 15 min were manually categorised by whether bedload was being transported. The recordings were categorised as 'Bedload Transport' if they were dominated by moving pebbles with more than 10 pebble hits over a 5-s window; however, if there was only the occasional pebble movement (<10 per 5 s), and it was dominated by turbulence noises the files were classified as 'No Bedload Transport'. The categorisation into the larger and smaller grains being transported is more ambiguous as it relied on an audible identification of a change in frequency; more could be done to look at the frequency characteristics of the hydroacoustic data, but this was not carried out for this work. For this work, we have categorised the smaller grains as 'Bedload Transport (phase 1)' and the larger grains as 'Bedload Transport (phase 2)'. It was assumed that the condition remained constant between each recording within a single transport phase, and therefore, the phases were assumed constant. The same researcher processed all the hydroacoustic data to minimise errors in the categorisation. At low water levels (∼0.6 m), the hydrophones are exposed and therefore do not record any river-related signals so are excluded from our analysis. Categorising the hydroacoustic data provides independent evidence when bedload transport took place that can be overlain on the seismic analysis to test the thresholds of entrainment for coarse bedload. It also provides a reliable independent measurement of bedload transport occurrence which is required to interpret hysteretic patterns observed in PSD versus water level data.

All stream gauge data, including those accessed from gauges SG1 and SG3, were linearly interpolated and resampled to 1-min intervals so that they could be combined with the geophone data analysed in minute long windows. Although the water level hydrographs during a high-flow event are fairly smooth and it is easy to interpolate between the 15-min samples, there may be some very small variability that is missed, particularly at base flows. However, 1-min interpolated data does not mask any of the 15-min recorded data. This also provided a richer database, as resampling the geophone data to 15-min intervals to match the original stream gauge data sample rate would potentially miss important information from the propagating flood waves.

3 | RESULTS

The results compare the co-located geophone and hydrophone data at site W_07 and H1, respectively, and geophone data collected at a

control site approximately 300 m from the river (E_06). This comparative analysis is supported by locally measured stream gauge data at SG2 (Figure 1c). The results describe the river-induced seismic signals at the two geophone sites, the observed transport thresholds over three successive high-flow events and the robustness of using hysteresis as a fingerprint of bedload transport.

3.1 | Comparison of the river site with the non-fluvial control site

First, we compare and contrast the geophone data recorded beside the river (W_07) and at the control site (E_06) in order to discriminate background environmental signals from those sourced from the river channel.

The water level time series and spectrograms derived from the geophone data at each site are plotted in Figure 4 for two different events. The November event is not shown because the control site geophone E_06 was not recording at this time. Prior to the water rising, all the spectrograms show vertical broadband streaks of high amplitude (approximately −140 to −145 dB), which correspond to the periods of rain that preceded the water level rises as we observed no snowmelt-only hydrological events (Figure 4c–f). Similarly, when the water level drops, it is likely that there will be less rain at the site,

and fewer vertical streaks on the spectrogram, as the water level would not be dropping if there was still significant rain across the catchment. This assumption does not necessarily hold true for large catchments as local conditions may vary from catchment wide conditions, such as rainfall patterns; however, our interpretation makes this assumption due to the relatively small catchment size. Some of these streaky broadband signals could also be a result of wind, but it is difficult to differentiate the two without further meteorological data as they tend to have similar characteristics and occupy similar frequency bands (Rindraharisaona et al., 2022).

In contrast to the control site, we see that the PSD time series measured at the river bank station, W_07, evolves as the water level changes. During periods of base level flow, when the water is low, the greatest power is recorded within a frequency range of approximately 5–35 Hz and is continuous, even during low flows prior to and following the large events. There is a sudden onset of higher frequency (30–80 Hz) high power seismic signals at W_07 recorded during the peak of the flood waves. During the highest water levels, these high power bands extend to higher frequencies, up to around 85 Hz, but once the river level drops towards base levels, these higher frequency signals become less dominant. These high-power, high-frequency signals are absent from the control site.

In order to develop further understanding of the subsequent, more detailed results (see below), we make some initial, first-order
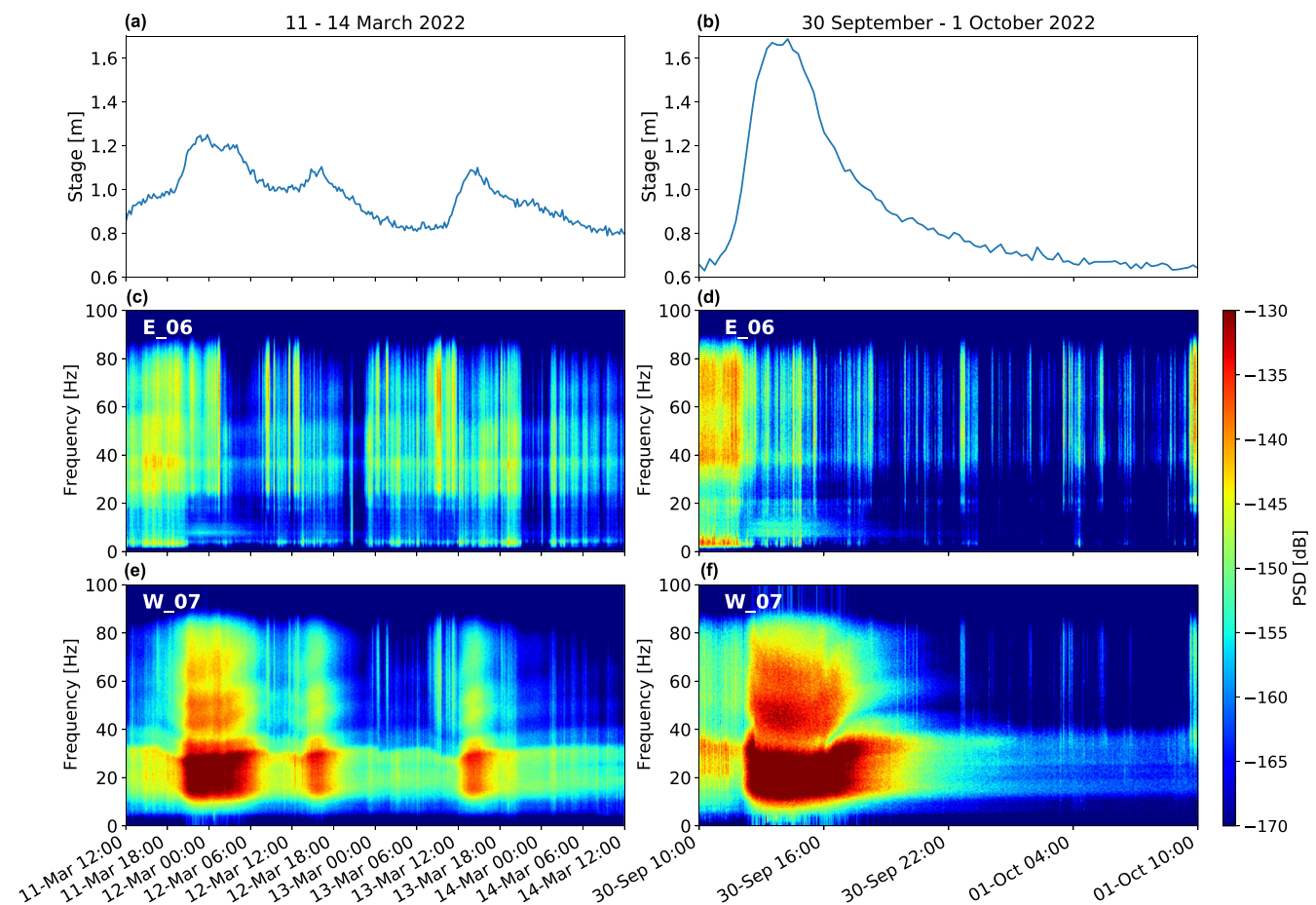

FIGURE 4 Data for two distinct high-flow events in March and September–October 2022, one in each column. Included in this plot are (a,b) the time series of the water level at SG2, (c,d) the spectrograms of the geophone data (in 1-min windows) at the control site to highlight environmental noise such as wind and rain and (e,f) the spectrograms of the geophones at the river site, which is dominated by signals of turbulence and sediment transport. [Color figure can be viewed at wileyonlinelibrary.com]

interpretations of the signals listed above. We interpret the constant seismic signal during low flows to be the background river signal (turbulence); this feature is absent at the control site. The frequency values we observe for this signal is slightly higher than those found in previous studies but is most likely a result of site characteristics. The band of higher frequency seismic noise during the event peaks suggests that there is a separate signal in addition to that derived from turbulence, which is not present when the water levels return back to base levels. The absence of these signals at the control site enforces the interpretation that these are river related signals to be determined by the hydroacoustic data. These comparisons allow us to identify the seismic signals that are induced by river-related processes, and specifically those induced by bedload transport, which are then used throughout the rest of this study to analyse transport thresholds and patterns.

Having documented the fingerprints of different physical processes within the time-frequency domain (Figure 4), we simplify the analysis by focusing on the 30–80 Hz band, as previous studies (e.g. Burtin et al., 2008; Roth et al., 2016; Turowski et al., 2015) have found that bedload transport produces signals at higher frequencies than turbulence, which going by our interpretation from Figure 4 would be >30 Hz. Specifically, in minute long windows shown in the spectrogram, we average the values of the power over the 50–60 Hz range for three distinct high-flow events to calculate a single scalar value at each time, which we refer to as the average power spectral density (aPSD) in the plots (see Section 2). This narrower frequency range was chosen as there was less influence from meteorological and turbulence seismic signals, making the bedload transport the strongest signal observed for those frequencies.

The aPSDs calculated using the selected 50–60 Hz frequency band highlight the use of site E_06 as a control site and the strength of the river-induced seismic signals recorded at W_07. At the control site, the PSD is dominated by the contributions from the broadband intermittent meteorological (wind and rain) signals. Consequently, the aPSD shows large scatter that is independent of the water level (Figure 5a,b). In contrast, the aPSD at the site beside the river, W_07, mirrors the variations in water level for all three events, showing a close parallel between the two (Figure 5c–e). The meteorological noise is still visible at site W_07 prior to the hydrological peaks, but the river-induced seismic noise is dominant above base water levels (~0.90–1.10 m) as turbulence increases and bedload begins to be mobilised.

3.2 | Analysis across three successive high-flow events

3.2.1 | Entrainment thresholds of coarse bedload

Using the hydrophone data, we classify whether bedload is being transported at site W_07, independent of the geophone data, and include this information on the water level and the concomitant aPSD plot (Figure 5c–e). The salmon and red-shaded regions in Figure 5c–e indicate when bedload is being transported, with the blue shading highlighting when only turbulence was observed and white regions when the hydrophone was exposed out of the water and therefore not recording any sound. All three of the high-flow events recorded the mobilisation of bedload during the peaks in water level, with the salmon colour, labelled 'Bedload transport (phase 1)' indicating the movement of bedload material. During the largest of the three events (the September–October event), there was also an audible shift in frequency of the recordings at the highest water level (>~1.50–1.60 m), which is shown in the reddish colour and labelled 'Bedload transport (phase 2)' in Figure 5d at the peak of the event, which lasted approximately 135 min. Recordings during the two transport phases and the only turbulence phase of the September–October event (Audio S1–S3) highlight the audible changes during these processes. This audible frequency drop in the hydroacoustic data from 'Bedload transport (phase 1)' to 'Bedload transport (phase 2)' from 13:15 to 15:30 on 30 September 2022 coincides with a shift to lower frequencies in the geophone data (Figure 4f and Supporting Information S2), where the lower frequency end of the high-amplitude seismic power dips from about 40 Hz to around 30 Hz at the same time as the peak of the hydrograph (30th September 14:00) and then rises back up following the peak. The gaps between the hydroacoustic categorisations in Figure 5c–h are due to the 15-min hydroacoustic sampling interval, resulting in a range of water levels at which mobilisation of coarse bedload starts. Here, this water level range is greater during the rising limb than the falling limb (Figure 5f–h) due to the rapid rate of increase in water level relative to the quarter-hourly hydrophone recordings compared to the gradually waning falling limb. Similar features would be observed in a rapidly decreasing flow; however, this was not the case in the events analysed here.

We compare the timing of onset of bedload transport with the time-equivalent water level to explore systematic changes in the threshold for initiation and arrest of motion across the three events. Figures 5 and 6 reveal that bedload mobilisation during the moderate March event consistently starts and stops at a water level of ~1.00 m. This is the case across all three daily peaks, labelled 1–3 in Figures 5c and 6b,c. However, during the largest September–October event, coarse bedload transport initiates at between 0.95 and 1.08 m, accounting for the uncertainty in the sampling period of the hydroacoustic data. The previously mentioned audible drop in frequency of the hydroacoustic data occurs between 1.50 and 1.59 m and continues throughout the peak (at 1.69 m) and falling limb and stops at around 1.39–1.44 m, labelled 'Bedload transport (phase 2)' in Figures 5 and 6. At this point on the falling limb, the audible frequency of the hydroacoustic recordings increases to a level similar to that of the initial mobilisation; bedload transport is sustained until the water level drops to ~0.87 m. The September–October event therefore had coarse bedload mobilisation initiating at ~1.00 m on the rising limb and ceasing at ~0.87 m on the falling limb. The third event in November is much like the early March event in that the mobilisation of bedload starts and stops at the same level on the rising and falling limb of the hydrograph. However, for this event, the entrainment threshold is now similar to that at the end of sediment transport in the September event at ~0.79–0.87 m.

3.2.2 | Hysteresis patterns

Consider the water level versus aPSD plots in Figure 5f–h and Figure 6a. These allow us to test the validity of the assumption that
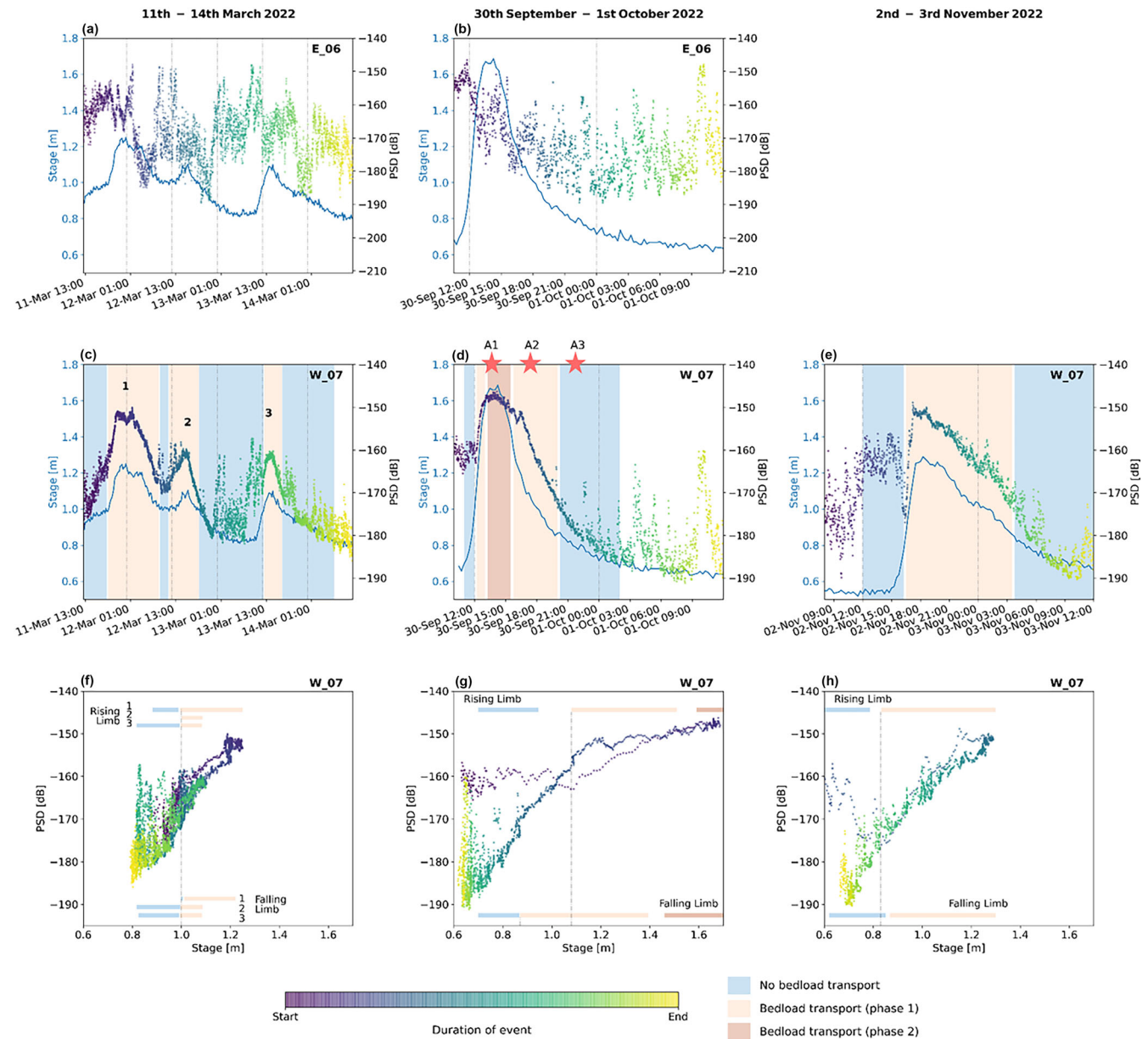
FIGURE 5 Plots summarising the time series of the water level (blue line) and seismic power averaged over the frequency range of 50–60 Hz (points coloured by time) for the three largest flow events in 2022. Each column displays a different event showing (a,b) the aPSD and water level time series for the control site highlighting the environmental noise around the water level peaks, (c–e) the aPSD time series for the river site layered on top of the independent classification of bedload transport activity using the hydroacoustic data (white shading shows gaps in the data or when the hydrophone was exposed; blue shows periods where the hydrophone records only turbulence; salmon shows when bedload transport starts (phase 1); and red shows when there is an audible shift to lower frequencies on the hydrophone interpreted to be mobilisation of larger grains during bedload transport (phase 2)) and (f,g,h) the PSD versus stage relationship with the hydrophone bedload transport classifications shown as bars for the rising and falling limbs of the hydrological peaks. Numbers 1, 2 and 3 in (c) and (f) are separate labels for each of the peaks in the March event. Red stars in (d) show the timings of the hydrophone recordings included in Audio S1–S3, labelled A1, A2 and A3. [Color figure can be viewed at wileyonlinelibrary.com]

hysteresis in the water level versus PSD is a reliable indicator of bedload transport processes.

As noted above, bedload transport occurred during all three events, which was independently evidenced through the hydroacoustic data. Looking at the water level versus aPSD plots, it is clear that both the March and November events have similar seismic signals on the rising and falling limbs of the hydrograph and show minimal signs of hysteresis despite independent evidence from the hydroacoustic data that bedload was actively being transported. There is slight clockwise hysteresis seen for the largest peak of the March event and for only the largest water levels (above

approximately 1.10 m) in the November event; however, there is no hysteresis for water levels below this despite there being evidence from the hydroacoustic data of bedload transport occurring from approximately 1.00 m in the March event and 0.79–0.87 m for the November event. The two events also show very similar aPSD values to each other on the rising and falling limbs, suggesting that the nature of coarse bedload transport may be comparable in both events.

In contrast, the aPSD analysed over the 50–60 Hz range in the larger September–October event does exhibit some anticlockwise hysteresis, but only between ~1.00 m and 1.40 m (Figure 5g). Until
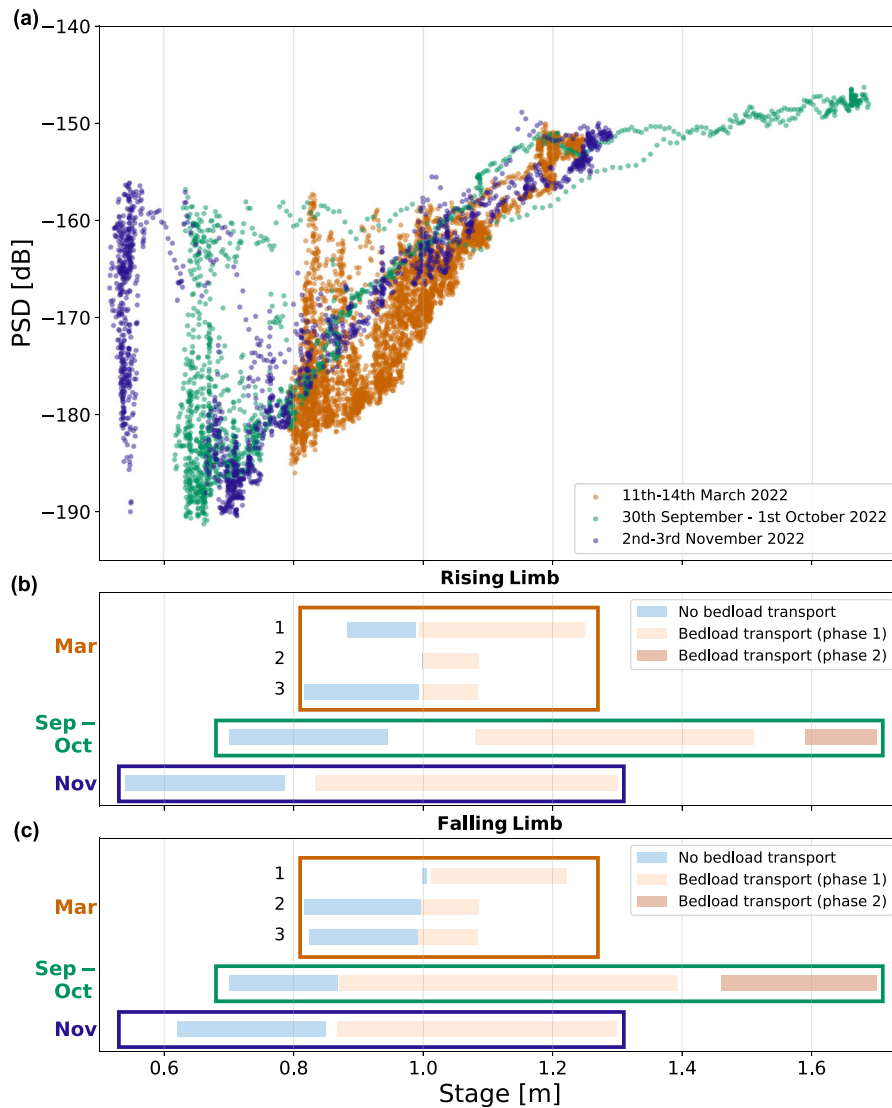
FIGURE 6 (a) Superposition of the PSD versus water level relationships for three distinct high-flow events to enable a clearer comparison of the similarities and differences between each event. (b) Bedload activity transitions from independent interpretation of hydroacoustic data that occurred on the rising limbs of flood peaks for all three events; note that for the March and September events, bedload started being transported at a water level of ~1.00–1.10 m, while transport during the November event initiated at a water level of ~0.80 m. (c) Bedload activity transitions from independent interpretation of hydroacoustic data that occurred on the falling limbs flood peaks for all three events; note that for the March event, bedload stopped being transported at a water level of ~1.00 m, while the arrest of bedload transport occurred at ~0.85 m for the September and November events. [Color figure can be viewed at wileyonlinelibrary.com]

around 12:00 on September 30 (at water levels <1.00 m), the aPSD is relatively constant at around −160 dB for this event while the rainfall dominates the seismic signal, as evidenced in Figure 5 d and discussed above in Section 3.1. Once the water level reaches ~1.00–1.10 m, the aPSD during the rising limb in Figure 5g appears to increase linearly until around 1.4 m at −148 dB where it levels off slightly until the peak of the event. During the falling limb, the decrease in aPSD is less steep until ~1.15 m, resulting in a sustained high aPSD, which can also be seen on Figure 5d where the aPSD remains close to peak levels for a short time after the peak even once the water level has begun to decrease. The largest variation in aPSD value between the rising and falling limb occurs at a water level of 1.2 m with the aPSD on the falling limb measuring approximately 7 dB higher than that on the rising limb. Below ~1.15 m the value of aPSD falls much more rapidly. The overlap of the aPSD at water levels greater than 1.4 m on the rising and falling limb coincides with the transport of 'Bedload transport (phase 2)' from the hydroacoustic data. These water levels exceed the levels of the March and November events, and so, this behaviour is not visible on Figure 5f,h.

In summary, the initial entrainment threshold water depth that was observed in March 2022 dropped by about 15%–20% (~1.00 m to ~0.80–0.85 m) following the September–October event peak, and this new lower threshold was maintained for the subsequent

November high-flow event. The March and November events show very little hysteresis, especially at lower water levels, whereas the larger September–October event shows a larger degree of anticlockwise hysteresis for water levels between ~1.00 m and 1.40 m (when bedload transport is observed to initiate) and then behaves linearly at water levels above 1.40 m. Due to the noise from meteorological signals at the initial stages of the high-flow events, it is difficult to identify any features in the seismic data that would indicate the initial transport of the coarse bedload, which is why the hydroacoustic data have proven very useful in this analysis.

4 | DISCUSSION

Due to the hazards and risks derived from the transport of coarse bedload, it is important to be able to monitor when and where the transport occurs within rivers. The seismic and hydroacoustic measurements at our field site in the alluvial River Feshie, recorded information on the mobilisation of coarse bedload. One of the strengths of our study is using three successive bedload transport events to assess the variations in thresholds of bedload entrainment and the water level versus seismic power hysteresis pattern variations through successive events.

We see the coarse bedload transport threshold changes following the largest of the three events suggesting that there is a dependence on the recent history of larger discharge events. Without evidence of dramatic changes in channel profile and bed structure, we speculate that there may have been a change to grain organisation and sorting on the bed following the largest event observed in 2022, which reduces the shear stress needed to entrain coarse bedload therefore allowing it to be more easily re-mobilised in a subsequent event (Jain et al., 2021). This could be a result of the very rapid fall in water level during the largest event compared to the March and November events inhibiting the bed to find a stable form (Luo et al., 2023; Masteller et al., 2019; Turowski et al., 2011). Since there were three other smaller water level peaks that only just exceeded the threshold of entrainment for the March event, it is possible these caused local reorganisation and strengthening of the bed up until the September–October event, at which point the significantly increased discharge could have cause a break in the local armour layer, leading to a deposition of unsorted material during the falling limb. The new 0.8 m threshold is exceeded a number of times between the September–October and November events and most likely resulted in movement of only the smallest grain sizes. This was therefore unlikely to contribute to the development of an armour layer, which would have caused an increase to the threshold for the November event, which is not observed in the data.

We hypothesise that, in the absence of a further large flow event like the September–October 2022 event, over cycles of moderate scale events, such as snow melt cycles or moderate rainfall events like the March and November events, the bed will progressively regain its strength as the clasts locally reorganise, bedforms stabilise, and the water level threshold for mobility will again rise to a higher value (Luo et al., 2023; Ockelford et al., 2019). This hypothesis is supported by the observation that in the initial March event, the daily rainfall plus snowmelt cycles were just sufficient to initiate the motion of bedload at their peak, suggesting that these moderate events have helped the system find a more stable configuration over time. Since events of a similar size to the March and November events are expected to happen approximately once every 5–6 months (Figure 3), there is potential for the river to undergo somewhat frequent local sorting of material before a large (approximately one in 1 year) event like the September–October event breaks through the sorted material and causes large amounts of resorting.

Prior to this study, hysteresis in the water level versus seismic PSD plot was viewed as an indicator of bedload transport processes, with a purely turbulence signal expected to have a distinct lack of hysteresis (Burtin et al., 2008; Hsu et al., 2011; Turowski et al., 2015). In our study, bedload was transported in all three events, as evidenced with the hydroacoustic data, but distinct hysteresis in the high-frequency seismic signal only occurred in the largest event when using co-located geophone and stream gauge data from SG2; thus, using hysteresis in the water level versus seismic data alone as an indicator of bedload transport processes is insufficient to analyse bedload transport events. Although a small degree of hysteresis was observed for the March and November events, it only occurred for the largest peak of the March event and only at water levels above approximately 1.10–1.20 m in the November event. During the smaller two peaks of the March event and the lower water levels of the November event, there were no hysteresis patterns observed despite the independent evidence from the hydroacoustic data that bedload transport did occur. This shows that hysteresis does not systematically correlate with the transport of bedload as evidenced from the independent hydroacoustic data.

Our findings are in agreement with Roth et al. (2017), who found that hysteresis may not be an effective measure of bedload transport as they identified that the seismic power tracks more closely to the changing water levels than the sediment transport rates measured using impact plate geophones. In addition to the general variation in PSD during the rising and falling limb of the September–October event, we also see a levelling off of the PSD for water levels above 1.40 m. One possible cause for a levelling off like this could be due to clipping of the waveforms when the amplitude of the recorded signal exceeds the upper limit of the geophones recording range, resulting in a loss of data. However, this is not the case here, and the observed behaviour is real (see Supporting Information S1). We speculate this levelling off in PSD to be most likely caused by the presence of a sheet flow of granular material, which would make it difficult to increase the frequency and magnitude of collisions with the bed (Palucis et al., 2018), thus reducing the seismic power measured in the high frequencies with increasing water level. Although there may be a limit on the grain-to-bed interactions during granular sheet flow, there will likely be increased grain-to-grain interaction, which is possible to record with the hydroacoustics. Further analysis into the frequency characteristics of hydroacoustic data would potentially shed some light on this.

In conjunction with the expected hysteresis at high frequencies, previous studies have suggested that analysing the low frequency band ($<\sim$1–30 Hz; e.g. Dietze & Gimbert, 2019; Chao et al., 2015; Burtin et al., 2008) can effectively isolate the turbulence signal. By focusing on this frequency range, it was suggested that a lack of hysteresis would be observed in the water level versus PSD plot (Tsai et al., 2012). However, findings from this study challenge these assumptions, especially in relation to the largest event analysed. Contrary to expectations, hysteresis is also observed in the lower frequency range that was interpreted to be the turbulence signal from the data in Figure 4, as shown in Supporting Information S1. This analysis may be complicated by the fact that bedload and turbulence can occupy overlapping frequency ranges, and therefore, discrimination of the frequency bands of interest is very important.

Looking forwards, long-term monitoring on this reach will allow observing a series of successive events with varying durations. This will provide a more comprehensive understanding of the factors influencing the threshold for bedload mobilisation. In particular, we can assess whether the bedload mobilisation threshold is primarily influenced by the magnitude of high-flow events, the duration of individual events or the periods between events. Furthermore, we can explore the relationship between these dynamics, the arrangement of the riverbed structure and the calculation of the entrainment threshold parameter, that is, the Shields stress.

5 | CONCLUSIONS

Developing a clear, robust methodology for understanding and digitally monitoring bedload transport and fluxes is fundamental for informing engineering and flood risk models, particularly with the

concerns regarding the increased magnitude and frequency of flood events as a result of climate change. The use of seismic sensors is a key step forward and provides the opportunity to monitor bedload transport in previously inaccessible conditions. Combining seismic data with other measurement techniques, such as hydroacoustic data as done in this study, allows for the independent interpretation of bedload mobilisation. This cross-checking of complementary methods increases confidence in identifying bedload transport. By studying three successive bedload transport events, we test for variations in the flow conditions in an alluvial river that characterise the onset and termination of particle entrainment, thereby exploring the presence of hysteresis in seismic data as a fingerprint of coarse bedload transport. Through the use of hydroacoustic data to independently characterise bedload transport, our study found that bedload transport occurred during all three events but that mobilisation initiated and terminated at different water levels. Notably, these entrainment thresholds were influenced by preceding events, with a discernible drop in the threshold flow depth of approximately 15%–20% following the largest of the three events. Our study also reveals that while hysteresis in seismic data, in relation to water level, can sometimes be indicative of bedload transport processes, the degree of hysteresis is dependent on the magnitude of the event and is not a definitive requirement. Being able to accurately distinguish between distinct seismic signals associated with bedload transport and water turbulence is crucial and will enable us to improve our ability to estimate bedload transport fluxes and gain deeper insights into the complex dynamics of alluvial rivers impacted by climate change. Our study shows the value in combining seismic and hydroacoustic data for long-term digital monitoring of bedload transport and suggests the possibility that this combination of data will allow us to identify different granular flow regimes in the field. Routine monitoring with such digital systems enables us to understand the systematic evolution in the onset of bedload transport and will be of direct use in calibrating widely used flood and bedload transport engineering models.

AUTHOR CONTRIBUTIONS

Bronwyn Matthews is the PhD student working on this project who has led the writing of this paper, done the data analysis and produced the figures. Undergraduate student Anna Smith undertook initial analysis of the hydrophone data, which informed our field deployment and classification using hydrophones. Mark Naylor designed the field experiment, led the project and co-wrote the paper. Hugh Sinclair contributed geomorphological expertise, co-wrote the paper and co-supervised Bronwyn Matthews. Andrew Black and Richard Williams provided expertise and experience in monitoring this catchment. Andrew Black also contributed wider meteorological and stream gauge data, and both Andrew Black and Richard Williams were involved in discussing results and editing the manuscript. Technology development that enabled the data to be collected was led by Calum Cuthill and Matthew Gervais. Michael Dietze provided expertise in the use of the seismic sensors for environmental monitoring and provided comments on the manuscript.

CONFLICT OF INTEREST STATEMENT

The authors have no conflict of interest in the materials or subject matter described in the manuscript.

DATA AVAILABILITY STATEMENT

Snippets of the hydroacoustic data are available as supplemental material, and all other data are available upon request to the authors.

PRE-PRINT STATEMENT

This paper is a non-peer-reviewed preprint submitted to EarthArXiv (doi: https://doi.org/10.31223/X5XX03) and has not yet been submitted to a journal for publication.

ORCID

Bronwyn Matthews https://orcid.org/0000-0003-0854-6107
Richard Williams https://orcid.org/0000-0001-6067-1947

REFERENCES

An, C., Parker, G., Hassan, M. & Fu, X. (2018) Can magic sand cause massive degradation of a gravel-bed river at the decadal scale? Shi-ting river, China. *Geomorphology*, 327, 147–158. Available from: https://doi.org/10.1016/j.geomorph.2018.10.026.

Bakker, M., Gimbert, F., Geay, T., Misset, C., Zanker, S. & Recking, A. (2020) Field application and validation of a seismic bedload transport model. *Journal of Geophysical Research*, 125(5), 22. Availabe from: https://doi.org/10.1029/2019JF005416.

Ballance, L.T., Pitman, R.L., Barlow, J., Pusser, T.D.A., Annamaria, I., Hayslip, C., et al. (2023) Acoustic recordings, biological observations, and genetic identification of a rare(?) beaked whale in the north Pacific: *Mesoplodon carlhubbsi*. *Marine Mammal Science*, 40(1), 123–142. Available from: https://doi.org/10.1111/mms.13059.

Barker, L., Hannaford, J., Muchan, K., Turner, S. & Parry, S. (2016) The winter 2015/2016 floods in the UK: a hydrological appraisal. *Weather*, 71(12), 324–333. Available from: https://doi.org/10.1002/wea.2822.

Barrière, J., Oth, A., Hostache, R. & Krein, A. (2015) Bed load transport monitoring using seismic observations in a low-gradient rural gravel bed stream: seismic monitoring of bedload transport. *Geophysical Research Letters*, 42(70), 2294–2301. Available from: https://doi.org/10.1002/2015GL063630.

Belleudy, P., Valette, A. & Graff, B. (2010) Monitoring of bedload in river beds with an hydrophone: first trials of signal analyses. In: Dittrich, A., Koll, K., Aberle, J. & Geisenhainer, Peter (Hg.): *River flow 2010*. Karlsruhe: Bundesanstalt für Wasserbau. S.1731-1740. https://hdl.handle.net/20.500.11970/99836.

Bogen, J. (1980) The hysteresis effect of sediment transport systems. *Norsk Geografisk Tidsskrift - Norwegian Journal of Geography*, 34(1), 45–54. Available from: https://doi.org/10.1080/00291958008545338.

Bountourakis, V., Elvander, F., & Pulkki, V. (2023) Using optimal mass transport in bearing-time records for underwater target localization and tracking. In Underwater Acoustic Conference and Exhibition

Series, 443-449. International Association for Hydro-Environment Engineering and Research.

Brasington, J., Rumsby, B.T. & McVey, R.A. (2000) Monitoring and modelling morphological change in a braided gravel-bed river using high resolution GPS-based survey. *Earth Surface Processes and Landforms: the Journal of the British Geomorphological Research Group*, 25(9), 973–990. Available from: https://doi.org/10.1002/1096-9837(200008)25:9<973::AID-ESP111>3.0.CO;2-Y.

Buffington, J.M. & Montgomery, D.R. (1997) A systematic analysis of eight decades of incipient motion studies, with special reference to gravel-bedded rivers. *Water Resources Research*, 33(8), 1993–2029. Available from: https://doi.org/10.1029/96WR03190.

Bunte, K. & Abt, S.R. (2005) Effect of sampling time on measured gravel bed load transport rates in a coarse-bedded stream. *Water Resources Research*, 41(11), Available from: https://doi.org/10.1029/2004WR003880.

Bunte, K., Abt, S.R., Potyondy, J.P. & Ryan, S.E. (2004) Measurement of coarse gravel and cobble transport using portable bedload traps. *Journal of Hydraulic Engineering*, 130(9), 879–893. Available from: https://doi.org/10.1061/(ASCE)0733-9429(2004)130:9(879.

Burtin, A., Bollinger, L., Vergne, J., Cattin, R. & Nábělek, J.L. (2008) Spectral analysis of seismic noise induced by rivers: a new tool to monitor spatiotemporal changes in stream hydrodynamics. *Journal of Geophysical Research*, 113(B5), 1-14. Available from: https://doi.org/10.1029/2007JB005034.

Burtin, A., Hovius, N., McArdell, B.W., Turowski, J.M. & Vergne, J. (2014) Seismic constraints on dynamic links between geomorphic processes and routing of sediment in a steep mountain catchment. *Earth Surface Dynamics*, 2(1), 21–33. Available from: https://doi.org/10.5194/esurf-2-21-2014.

Burtin, A., Vergne, J., Rivera, L. & Dubernet, P. (2010) Location of river-induced seismic signal from noise correlation functions: location of river seismic signal. *Geophysical Journal International*, 182(3), 1161–1173. Available from: https://doi.org/10.1111/j.1365-246X.

Chao, W.-A., Wu, Y.-M., Zhao, L., Tsai, V.C. & Chen, C.-H. (2015) Seismologically determined bedload flux during the typhoon season. *Scientific Reports*, 5(1), 8261. Available from: https://doi.org/10.1038/srep08261.

Chełmicki, W. & Krzemień, K. (1999) Channel typology for the river Feshie in the Cairngorm Mts, Scotland. In: *Prace Geograficzne*. London: Nature Publishing Group.

Church, M. (2006) Bed material transport and the morphology of alluvial river channels. *Annual Review of Earth and Planetary Sciences*, 34(1), 325–354. Available from: https://doi.org/10.1146/annurev.earth.33.092203.122721.

Church, M., Hassan, M.A. & Wolcott, J.F. (1998) Stabilizing self-organized structures in gravelbed stream channels: field and experimental observations. *Water Resources Research*, 34(11), 3169–3179. Available from: https://doi.org/10.1029/98WR00484.

Cox, J.R., Huismans, Y., Knaake, S.M., Leuven, J.R.F.W., Vellinga, N.E., van der Vegt, M., et al. (2021) Anthropogenic effects on the contemporary sediment budget of the lower Rhine-Meuse delta channel network. *Earth's Future*, 9(7), 1-22. Available from: https://doi.org/10.1029/2020EF001869.

Dean, T. (2018) The seismic signature of rain. *ASEG Extended Abstracts*, 2018(1), 1–8. Available from: https://doi.org/10.1071/ASEG2018abP068.

Dey, S. (2014) Fluvial hydrodynamics. In: *GeoPlanet: earth and planetary sciences*. Berlin, Heidelberg: Springer Berlin Heidelberg. https://doi.org/10.1007/978-3-642-19062-9.

Dietze, M. & Gimbert, F. (2019) The seismic view on sediment laden ephemeral flows – modelling of ground motion data for fluid and bedload dynamics in the Arroyo de los Piños. p. 10.

Dietze, M., Lagarde, S., Halfi, E., Laronne, J.B. & Turowski, J.M. (2019) Joint sensing of bedload flux and water depth by seismic data inversion. *Water Resources Research*, 55(11), 9892–9904. Available from: https://doi.org/10.1029/2019WR026072.

Downs, P.W., Soar, P.J. & Taylor, A. (2016) The anatomy of effective discharge: the dynamics of coarse sediment transport revealed using continuous bedload monitoring in a gravel-bed river during a very wet year: dynamics of coarse sediment transport using continuous monitoring. *Earth Surface Processes and Landforms*, 41(2), 147–161. Available from: https://doi.org/10.1002/esp.3785.

Ferguson, R.I. & Werritty, A. (1983) Bar development and channel changes in the gravelly river Feshie, Scotland. In: Collinson, J.D. & Lewin, J. (Eds.) *Modern and ancient fluvial systems*. Oxford, UK: Blackwell Publishing Ltd., pp. 181–193 https://doi.org/10.1002/9781444303773.ch14.

Gaeuman, D. (2010) Mechanics of bedload rating curve shifts and bedload hysteresis in the Trinity river, California.

Geay, T., Zanker, S., Misset, C. & Recking, A. (2020) Passive acoustic measurement of bedload transport: toward a global calibration curve? *Journal of Geophysical Research: Earth Surface*, 125(8), 1-19. Available from: https://doi.org/10.1029/2019JF005242.

Gimbert, F., Tsai, V.C. & Lamb, M.P. (2014) A physical model for seismic noise generation by turbulent flow in rivers. *Journal of Geophysical Research: Earth Surface*, 119(10), 2209–2238. Available from: https://doi.org/10.1002/2014JF003201.

Gomez, B. & Soar, P.J. (2022) Bedload transport: beyond intractability. *Royal Society Open Science*, 9(3), 211932. Available from: https://doi.org/10.1098/rsos.211932.

Habersack, H.M., Nachtneb El, H.P. & Laronne, J.B. (2001) The continuous measurement of bedload discharge in a large alpine gravel bed river. *Journal of Hydraulic Research*, 39(2), 125–133. Available from: https://doi.org/10.1080/00221680109499813.

Hassan, M.A., Egozi, R. & Parker, G. (2006) Experiments on the effect of hydrograph characteristics on vertical grain sorting in gravel bed rivers. *Water Resources Research*, 42(9), 1-15. Available from: https://doi.org/10.1029/2005WR004707.

Hauer, C., Leitner, P., Unfer, G., Pulg, U., Habersack, H. & Graf, W. (2018) The role of sediment and sediment dynamics in the aquatic environment. In: Schmutz, S. & Sendzimir, J. (Eds.) *Riverine ecosystem management: science for governing towards a sustainable future*. Cham: Springer International Publishing, pp. 151–169 https://doi.org/10.1007/978-3-319-73250-3_8.

Holmes, R. (2010) Measurement of bedload transport in sand-bed rivers: a look at two indirect sampling methods. p. 17.

Hsu, L., Finnegan, N.J. & Brodsky, E.E. (2011) A seismic signature of river bedload transport during storm events. *Geophysical Research Letters*, 38(13), 1-6. Available from: https://doi.org/10.1029/2011GL047759.

Jain, R., Tschisgale, S. & Fröhlich, J. (2021) Impact of shape: DNS of sediment transport with non-spherical particles. *Journal of Fluid Mechanics*, 916, 1-15. Available from: https://doi.org/10.1017/jfm.2021.214.

Kothyari, U.C. & Jain, R.K. (2008) Influence of cohesion on the incipient motion condition of sediment mixtures. *Water Resources Research*, 44(4), 1-15. Available from: https://doi.org/10.1029/2007WR006326.

Kuhnle, R.A. (1992) Bed load transport during rising and falling stages on two small streams. *Earth Surface Processes and Landforms*, 17(2), 191–197. Available from: https://doi.org/10.1002/esp.3290170206.

Lagarde, S., Dietze, M., Gimbert, F., Laronne, J.B., Turowski, J.M. & Halfi, E. (2021) Grain-size distribution and propagation effects on seismic signals generated by bedload transport. *Water Resources Research*, 57(4), 1-20. Available from: https://doi.org/10.1029/2020WR028700.

Lee, K.T., Liu, Y.-L. & Cheng, K.-H. (2004) Experimental investigation of bedload transport processes under unsteady flow conditions. *Hydrological Processes*, 18(13), 2439–2454. Available from: https://doi.org/10.1002/hyp.1473.

Lisle, T.E. & Madej, M.A. (1992) Spatial variation in armouring in a channel with high sediment supply. In: *Dynamics of gravel-bed rivers*. Chichester, UK: John Wiley and Sons, pp. 277–293.

Luo, M., Jiang, Y., Wang, S., Liu, X. & Huang, E. (2023) The effect of stress history on fluctuation of bedload transport rate and bed topography in gravel-bed streams. *Journal of Hydrology*, 616, 128732. Available from: https://doi.org/10.1016/j.jhydrol.2022.128732.

Mao, L. (2012) The effect of hydrographs on bed load transport and bed sediment spatial arrangement. *Journal of Geophysical Research: Earth*

Surface, 117(F3), 1-16. Available from: https://doi.org/10.1029/2012JF002428.

Mao, L., Dell'Agnese, A., Huincache, C., Penna, D., Engel, M., Niedrist, G., et al. (2014) Bedload hysteresis in a glacier-fed mountain river. *Earth Surface Processes and Landforms*, 39(7), 964–976. Available from: https://doi.org/10.1002/esp.3563.

Masteller, C., Finnegan, N., Turowski, J., Yager, E. & Rickenmann, D. (2019) History-dependent threshold for motion revealed by continuous bedload transport measurements in a steep mountain stream. *Geophysical Research Letters*, 46(5), 2583–2591. Available from: https://doi.org/10.1029/2018GL081325.

Ockelford, A. & Haynes, H. (2013) The impact of stress history on bed structure. *Earth Surface Processes and Landforms*, 38(7), 717–727. Available from: https://doi.org/10.1002/esp.3348.

Ockelford, A., Woodcock, S. & Haynes, H. (2019) The impact of inter-flood duration on non-cohesive sediment bed stability. *Earth Surface Processes and Landforms*, 44(14), 2861–2871. Available from: https://doi.org/10.1002/esp.4713.

Osborne, W.A., Hodge, R., Love, G., Hawkin, P. & Hawkin, R. (2021) Babbling brook to thunderous torrent: using sound to monitor river stage. *Earth Surface Processes and Landforms*, 46(13), 2656–2670. Available from: https://doi.org/10.1002/esp.5199.

Palucis, M.C., Ulizio, T., Fuller, B. & Lamb, M.P. (2018) Intense granular sheetflow in steep streams. *Geophysical Research Letters*, 45(11), 5509–5517. Available from: https://doi.org/10.1029/2018GL077526.

Pitlick, J., Cui, Y. & Wilcock, P. (2009) Manual for computing bed load transport using BAGS (bedload assessment for gravel-bed streams) software.

Pretzlav, K., Johnson, J. & Bradley, D.N. (2020) Smartrock transport in a mountain stream: bedload hysteresis and changing thresholds of motion. *Water Resources Research*, 56(11), e2020WR028150. Available from: https://doi.org/10.1029/2020WR028150.

Reid, I., Frostick, L.E. & Layman, J.T. (1985) The incidence and nature of bedload transport during flood flows in coarse-grained alluvial channels. *Earth Surface Processes and Landforms*, 10(1), 33–44. Available from: https://doi.org/10.1002/esp.3290100107.

Rickenmann, D. (1991) Hyperconcentrated flow and sediment transport at steep slopes. *Journal of Hydraulic Engineering*, 117(11), 1419–1439. Available from: https://doi.org/10.1061/(ASCE)0733-9429(1991)117:11(1419.

Rickenmann, D., Ammann, L., Nicollier, T., Boss, S., Fritschi, B., Antoniazza, G., et al. (2022) Comparison of calibration characteristics of different acous793 tic impact systems for measuring bedload transport in mountain streams. *Earth Surface Dynamics*, 10, 1165–1166, 1183. Available from: https://doi.org/10.5194/esurf-10-1165-2022.

Rickenmann, D., Turowski, J.M., Fritschi, B., Wyss, C., Laronne, J., Barzilai, R., et al. (2014) Bedload transport measurements with impact plate geophones: comparison of sensor calibration in different gravel-bed streams. *Earth Surface Processes and Landforms*, 39(7), 928–942. Available from: https://doi.org/10.1002/esp.3499.

Rindraharisaona, E.J., Réchou, A., Fontaine, F.R., Barruol, G., Stamenoff, P., Boudevillain, B., et al. (2022) Seismic signature of rain and wind inferred from seismic data. *Earth and Space Science*, 9(10), 1-16. Available from: https://doi.org/10.1029/2022EA002328.

Roth, D.L., Brodsky, E.E., Finnegan, N.J., Rickenmann, D., Turowski, J.M. & Badoux, A. (2016) Bed load sediment transport inferred from seismic signals near a river. *Journal of Geophysical Research: Earth Surface*, 121(4), 725–747. Available from: https://doi.org/10.1002/2015JF003782.

Roth, D.L., Finnegan, N.J., Brodsky, E.E., Rickenmann, D., Turowski, J.M., Badoux, A., et al. (2017) Bed load transport and boundary roughness changes as competing causes of hysteresis in the relationship between river discharge and seismic amplitude recorded near a steep mountain stream. *Journal of Geophysical Research: Earth Surface*, 122(5), 1182–1200. Available from: https://doi.org/10.1002/2016JF004062.

Schmandt, B., Aster, R.C., Scherler, D., Tsai, V.C. & Karlstrom, K. (2013) Multiple fluvial processes detected by riverside seismic and infrasound monitoring of a controlled flood in the grand canyon. *Geophysical Research Letters*, 40(18), 4858–4863. Available from: https://doi.org/10.1002/grl.50953.

Schmandt, B., Gaeuman, D., Stewart, R., Hansen, S.M., Tsai, V.C. & Smith, J. (2017) Seismic array constraints on reach-scale bedload transport. *Geology*, 45(4), 299–302. Available from: https://doi.org/10.1130/G38639.1.

Stark, K., Cadol, D., Varyu, D., Halfi, E. & Laronne, J.B. (2024) Strengths and weaknesses of acoustic pipe microphone systems in ephemeral, sandy, gravel-bed rivers. *Earth Surface Processes and Landforms*, 49(4), 1383–1396. Available from: https://doi.org/10.1002/esp.5774.

Thorne, P.D. (2014) An overview of underwater sound generated by interparticle collisions and its application to the measurements of coarse sediment bedload transport. *Earth Surface Dynamics*, 2(2), 531–543. Available from: https://doi.org/10.5194/esurf-2-531-2014.

Tsai, V.C., Minchew, B., Lamb, M.P. & Ampuero, J.-P. (2012) A physical model for seismic noise generation from sediment transport in rivers. *Geophysical Research Letters*, 39(2), 1-6. Available from: https://doi.org/10.1029/2011GL050255.

Turowski, J.M., Badoux, A. & Rickenmann, D. (2011) Start and end of bedload transport in gravel-bed streams. *Geophysical Research Letters*, 38(4), 1-5. Available from: https://doi.org/10.1029/2010GL046558.

Turowski, J.M., Böckli, M., Rickenmann, D. & Beer, A.R. (2013) Field measurements of the energy delivered to the channel bed by moving bed load and links to bedrock erosion. *Journal of Geophysical Research: Earth Surface*, 118(4), 2438–2450. Available from: https://doi.org/10.1002/2013JF002765.

Turowski, J.M., Wyss, C.R. & Beer, A.R. (2015) Grain size effects on energy delivery to the streambed and links to bedrock erosion. *Geophysical Research Letters*, 42(6), 1775–1780. Available from: https://doi.org/10.1002/2015GL063159.

Vore, M.E., Bartholomaus, T.C., Winberry, J.P., Walter, J.I. & Amundson, J.M. (2019) Seismic tremor reveals spatial organization and temporal changes of subglacial water system. *Journal of Geophysical Research: Earth Surface*, 124(2), 427–446. Available from: https://doi.org/10.1029/2018JF004819.

Welch, P. (1967) The use of fast Fourier transform for the estimation of power spectra: a method based on time averaging over short, modified periodograms. *IEEE Transactions on Audio and Electroacoustics*, 15(2), 70–73. Available from: https://doi.org/10.1109/TAU.1967.1161901.

Wilcock, P. & Crowe, J.C. (2003) Surface-based transport model for mixed-size sediment. *Journal of Hydraulic Engineering*, 129(2), 120–128. Available from: https://doi.org/10.1061/(ASCE)0733-9429(2003)129:2(120.

Wilcock, W., Webb, S. & Bjarnason, I. (1999) The effect of local wind on seismic noise near 1 Hz at the MELT site and in Iceland. *Bulletin of the Seismological Society of America*, 89(6), 1543–1557. Available from: https://doi.org/10.1785/BSSA0890061543.

Wolman, M.G. (1954) A method of sampling coarse river-bed material. *Eos, Transactions American Geophysical Union*, 35(6), 951–956. Available from: https://doi.org/10.1029/TR035i006p00951.

SUPPORTING INFORMATION

Additional supporting information can be found online in the Supporting Information section at the end of this article.

How to cite this article: Matthews, B., Naylor, M., Sinclair, H., Black, A., Williams, R., Cuthill, C. et al. (2024) Sounding out the river: Seismic and hydroacoustic monitoring of bedload transport. *Earth Surface Processes and Landforms*, 49(12), 3840–3854. Available from: https://doi.org/10.1002/esp.5940